Physica Scripta

PAPER

Gamma-ray spectroscopy of ^{55}Sc

R Zidarova[1], M L Cortés[2], V Werner[1,3], P Koseoglou[1], N Pietralla[1], P Doornenbal[2], A Obertelli[1,2,4], T Otsuka[5], Y Tsunoda[5], Y Utsuno[5,6], N L Achouri[7], H Baba[2], F Browne[2], D Calvet[4], F Château[4], S Chen[2,8,9], N Chiga[2], A Corsi[4], A Delbart[4], J-M Gheller[4], A Giganon[4], A Gillibert[4], C Hilaire[4], T Isobe[2], T Kobayashi[10], Y Kubota[2,11], V Lapoux[4], H N Liu[1,4,12], T Motobayashi[2], I Murray[2,13], H Otsu[2], V Panin[2], N Paul[4], W Rodriguez[2,14,15], H Sakurai[2,16], M Sasano[2], D Steppenbeck[2], L Stuhl[4,17], Y L Sun[1,4], Y Togano[18], T Uesaka[2], K Wimmer[2,15], K Yoneda[2], O Aktas[12], T Aumann[1,19], L X Chung[20], F Flavigny[13], S Franchoo[13], I Gasparic[1,2,21], R-B Gerst[22], J Gibelin[7], K I Hahn[23,24], D Kim[2,23,24], T Koiwai[16], Y Kondo[25], J Lee[8], C Lehr[1], B D Linh[20], T Lokotko[8], M MacCormick[13], K Moschner[22], T Nakamura[25], S Y Park[23,24], D Rossi[1], E Sahin[26], P-A Söderström[1], D Sohler[17], S Takeuchi[25], H Toernqvist[1,19], V Vaquero[27], V Wagner[1], S Wang[28], X Xu[8], H Yamada[25], D Yan[28], Z Yang[2], M Yasuda[25] and L Zanetti[1]

[1] Institut für Kernphysik,Technische Universität Darmstadt, Schlossgartenstraße 9, 64289 Darmstadt, Germany
[2] RIKEN Nishina Center, 2-1 Hirosawa, Wako, Saitama 351-0198, Japan
[3] Helmholtz Forschungsakademie Hessen für FAIR (HFHF), Germany
[4] IRFU, CEA, Université Paris-Saclay, F-91191 Gif-sur-Yvette, France
[5] Center for Nuclear Study, University of Tokyo, Hongo, Bunkyo, Tokyo 113-0033, Japan
[6] Advanced Science Research Center, Japan Atomic Energy Agency, Tokai, Ibaraki 319-1195, Japan
[7] LPC Caen, Normandie Univ, ENSICAEN, UNICAEN, CNRS/IN2P3, F-14000 Caen, France
[8] Department of Physics, The University of Hong Kong, Pokfulam, Hong Kong, People's Republic of China
[9] State Key Laboratory of Nuclear Physics and Technology, Peking University, Beijing 100871, People's Republic of China
[10] Department of Physics, Tohoku University, Sendai 980-8578, Japan
[11] Center for Nuclear Study, University of Tokyo, RIKEN campus, Wako, Saitama 351-0198, Japan
[12] Department of Physics, Royal Institute of Technology, SE-10691 Stockholm, Sweden
[13] Université Paris-Saclay, CNRS/IN2P3, IJCLab, F-91405 Orsay cedex, France
[14] Pontificia Universidad Javeriana, Facultad de Ciencias, Departamento de Física, Bogotá, Colombia
[15] Universidad Nacional de Colombia, Sede Bogotá, Facultad de Ciencias, Departamento de Física, Bogotá 111321, Colombia
[16] Department of Physics, University of Tokyo, 7-3-1 Hongo, Bunkyo, Tokyo 113-0033, Japan
[17] HUN-REN Institute for Nuclear Research, Atomki, P.O. Box 51, Debrecen H-4001, Hungary
[18] Department of Physics, Rikkyo University, 3-34-1 Nishi-Ikebukuro, Toshima, Tokyo 172-8501, Japan
[19] GSI Helmholtzzentrum für Schwerionenforschung GmbH, Planckstr. 1, 64291 Darmstadt, Germany
[20] Institute for Nuclear Science & Technology, VINATOM, 179 Hoang Quoc Viet, Cau Giay, Hanoi, Vietnam
[21] Rudjer Bošković Institute, Bijenička cesta 54, 10000 Zagreb, Croatia
[22] Institut für Kernphysik, Universität zu Köln, D-50937 Cologne, Germany
[23] Ewha Womans University, Seoul 03760, Republic of Korea
[24] Institute for Basic Science, Daejeon 34126, Republic of Korea
[25] Department of Physics, Tokyo Institute of Technology, 2-12-1 O-Okayama, Meguro, Tokyo, 152-8551, Japan
[26] Department of Physics, University of Oslo, N-0316 Oslo, Norway
[27] Instituto de Estructura de la Materia, CSIC, E-28006 Madrid, Spain
[28] Institute of Modern Physics, Chinese Academy of Siences, Lanzhou 730000, People's Republic of China

E-mail: rzidarova@ikp.tu-darmstadt.de

Abstract

The $N = 34$ isotope ^{55}Sc has been investigated using in-beam γ-ray spectroscopy at the RIKEN Radioactive Isotope Beam Factory. Spectra from the direct (p, pn) reaction as well as indirect reaction channels have been investigated. γ rays with energies 496(10), 570(12), 682(14), 1510(30), 1780(36), 2345(57) and 2470(50) keV have been observed. A level scheme was constructed based on $\gamma\gamma$ coincidence analysis and relative intensities. The results have been compared to the level scheme already reported in literature, as well as to large-scale shell model calculations in the $sd - pf$ model space. A new level at 1510keV, decaying directly to the ground state, has been proposed and spin-parity $J^{\pi} = 7/2^-$ was tentatively assigned. The effect of including the $\nu g_{9/2}$ orbital is discussed. It can be concluded that the main low-energy properties of ^{55}Sc seem to be included in the original $sd - pf$ model space.

1. Introduction

Recent studies have shown the disappearance of the well-known shell-model 'magic numbers' and the appearance of new ones in nuclei very far from stability [1–3]. Those structural changes can be explained by the differences in the energy and ordering of single-particle orbitals with respect to stable isotopes. A particularly interesting example is the appearance of subshell closures at $N = 32$ and $N = 34$ around the Ca isotopes, among others.

Evidence for the $N = 32$ and $N = 34$ subshell closures was experimentally observed in the Ca isotopes via measurements of energies of first excited 2^+ states [2, 4], masses [3, 5], and knockout cross sections [6, 7]. Their existence has been investigated in the context of tensor-force-driven shell evolution in the pf shell [8, 9], in which weakening of the attractive proton-neutron interaction is observed when protons are removed from the $\pi f_{7/2}$ orbital, causing the $\nu f_{5/2}$ orbital to shift up in energy with respect to the $\nu p_{1/2}$ orbital. Moreover, a lot of effort has been dedicated to address the $N = 34$ subshell closure in the effective shell model framework [10] and with coupled-cluster theory [11].

The evolution of these subshell closures has also been studied in nuclei above and below Ca. The $N = 32$ subshell closure has been confirmed above $Z = 20$ for ^{54}Ti [12, 13] and ^{56}Cr [14–16], and below $Z = 20$ for ^{50}Ar [17, 18]. The $N = 34$ subshell closure has been confirmed below Ca in ^{52}Ar [19], however no indication of its existence has been found for ^{56}Ti [13, 20–22] and ^{58}Cr [15, 16]. Those results have sparked interest to study the Sc isotopes, located between the Ca and Ti isotopic chains, since information on the evolution of the proton orbitals can reveal the nature of the observed magicity [23, 24].

In the Sc isotopic chain mass measurements have been performed in recent years [21, 22, 25], concluding that the $N = 34$ subshell closure does not extend to the Sc isotopes. The first spectroscopy of ^{55}Sc, at the $N = 34$ shell closure, has been reported in [26]. The first excited state was found to be at an energy of 695(5) keV, based on γ-ray spectroscopy following ^{9}Be(^{56}Ti,^{55}Sc+γ)X and ^{9}Be(^{55}Sc,^{55}Sc+γ) reactions. Additional γ rays were measured and placed in a tentative level scheme [26]. Those results were compared to large-scale shell model calculations in the $sd - pf$ model space, which adopted the full sd and pf shells for protons and neutrons. The theory suggests a first excited state with spin-parity $3/2^-$ at around 700 keV. Based on this good agreement with the calculation, a rapid weakening of the $N = 34$ subshell closure has been concluded for $Z = 21$. Furthermore, a more recent study [27] exploring the effects of the different components of the proton-neutron GXPF1B interaction (with modification listed in [27]) also reproduces the available experimental data and recognizes that the low energy of the $3/2^-$ state is caused by the weakening of the $N = 34$ semimagic gap and not due to a decrease in the $Z = 28$ magic shell gap.

To further explore the shell evolution towards the $N = 40$ pf-shell closure we have performed an experiment to study neutron-rich isotopes in that mass region. Here we report the results from γ-ray spectroscopy of the $N = 34$ isotope ^{55}Sc.

2. Experiment

The experiment was performed at the Radioactive Isotope Beam Factory, operated by the RIKEN Nishina Center and the Center for Nuclear Study of the University of Tokyo. A primary beam of ^{70}Zn was accelerated to 345 MeV/u and impinged on a 10-mm-thick ^{9}Be target. The cocktail beam was separated and identified using the $B\rho - \Delta E - TOF$ [28] technique at the BigRIPS two-stage magnetic separator [29]. The velocity was obtained by measuring the time of flight (TOF), provided by the difference in time signals from three plastic scintillators, located at focal planes F3, F5, and F7. The magnetic rigidity, B_ρ, was calculated using position and angle measurements in parallel plate avalanche counters at F3, F5, and F7 [30], together with optical matrices for the ion paths in the magnetic field. The atomic number Z was calculated using the Bethe-Bloch formula for the energy loss ΔE of the particles in an ionization chamber [31]. The incoming particle identification, gated on outgoing ^{55}Sc ions, can be seen in figure 1(a).

A liquid hydrogen target (LH2) of 150 mm, surrounded by a Time Projection Chamber (TPC), was used to induce proton-knockout reactions. This device, called MINOS [32], could provide information on the reaction vertex in the LH2 target with a precision of 5mm (FWHM) and had a proton detection efficiency of over 90% for $(p, 2p)$ reactions [32, 33]. After the reaction with the LH2 target, outgoing ions were identified using the SAMURAI dipole magnet [34]. A similar $B\rho - \Delta E - TOF$ method was used for the particle identification. The ions' trajectories were reconstructed using position measurements in drift chambers [35], located upstream and downstream of the magnet. The magnetic rigidity $B\rho$ and the flight length, FL, were obtained using a GEANT4 [36] simulation of the particle trajectories in the magnetic field of SAMURAI. The velocity of the particles was determined using the simulated flight length and the TOF measured between a plastic scintillator, placed before
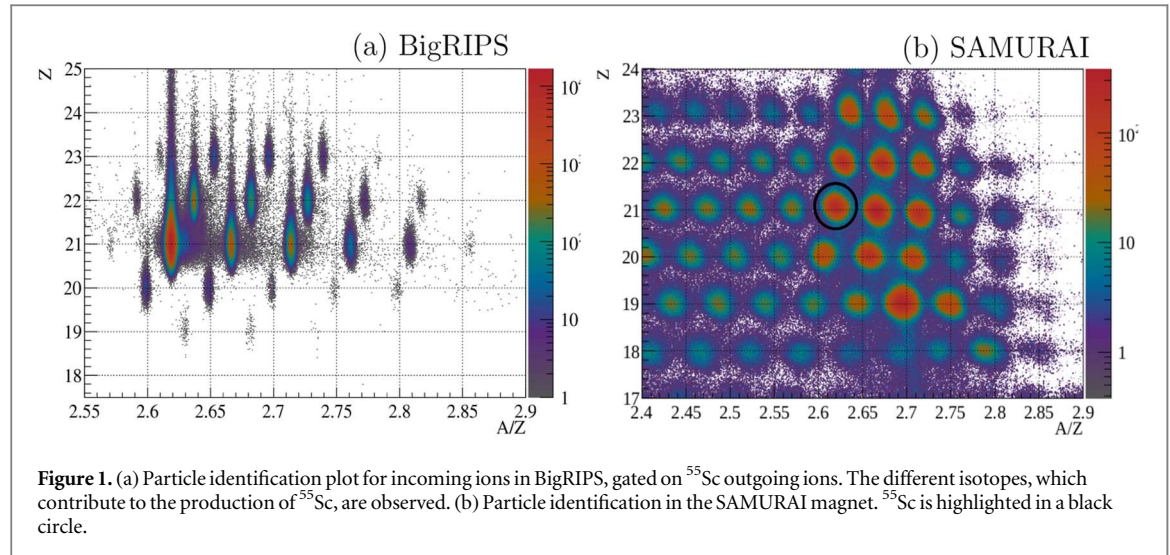
Figure 1. (a) Particle identification plot for incoming ions in BigRIPS, gated on ^{55}Sc outgoing ions. The different isotopes, which contribute to the production of ^{55}Sc, are observed. (b) Particle identification in the SAMURAI magnet. ^{55}Sc is highlighted in a black circle.

Table 1. Summary of different reaction channels producing ^{55}Sc. Total number of events in each channel, efficiency of MINOS (ϵ_{MINOS}), as well as inclusive cross sections (σ_{inc}) are listed. The transmission and efficiency of MINOS were used to obtain the inclusive cross sections for each channel.

Reaction	Events	ϵ_{MINOS}(%)	σ_{inc}(mb)
^{56}Sc(p,pn)^{55}Sc	122 684	71(1)	38.6(10)
^{57}Sc($p,p2n$)^{55}Sc	4759	68(1)	30.4(8)
^{58}Sc($p,p3n$)^{55}Sc	1754	69(1)	51.9(20)
^{58}Ti($p,2p2n$)^{55}Sc	12 184	93(2)	5.8(3)
^{59}Ti($p,2p3n$)^{55}Sc	19 239	90(1)	7.9(2)
^{60}Ti($p,2p4n$)^{55}Sc	11 581	87(1)	10.9(2)

the target, and a 24-segment Hodoscope. The atomic number was determined by measuring the energy loss of the fragments in the Hodoscope. The outgoing particle identification can be seen in figure 1(b).

For the γ-ray detection, the DALI2$^+$ [37, 38] array was used. It consisted of 226 NaI(Tl) detectors, which were arranged in 10 layers and offer full-energy peak efficiency of 30% at 1 MeV and energy resolution of 11% for a moving source with velocity of 0.6c. Energy calibration was done using standard calibration sources - ^{60}Co, ^{88}Y, ^{133}Ba, and ^{137}Cs. GEANT4 simulations were performed to obtain the response function of the array.

3. Results

^{55}Sc was populated by direct and indirect reactions. The statistics of all channels are listed in table 1. Precise Doppler correction was performed on the detected γ rays using the velocity of the fragments reconstructed at the vertex position and the angle between the vertex position and the DALI2$^+$ crystal where the γ ray was detected. To improve the peak-to-total ratio, an add-back procedure was performed by adding up the energies of γ rays, interacting within 15 cm radius. An energy threshold of 250 keV was applied at low energies and a time gate of $(-5;+7)$ ns was used to reduce background. Figure 2 shows the γ-ray spectra obtained from the ^{56}Sc(p,pn)^{55}Sc reaction with γ-ray multiplicity (a) $M_\gamma \leqslant 5$ and (b) $M_\gamma = 1$. The $M_\gamma = 1$ spectrum has been used to highlight the γ rays decaying directly to the ground state and to suppress Compton background. The $M_\gamma \leqslant 5$ spectrum has been chosen as the γ-ray intensities saturate at that point, while the atomic background does not and therefore this multiplicity condition allows for the best peak-to-background ratio without sacrificing valid events in the γ-ray peaks. Five distinct peaks can be observed at energies 570(12), 682(14), 1510(30), 1780(36) and 2470(50) keV. Two weaker transitions at 496(10) and 2345(57) keV were also observed. The 2345- and 2470-keV transitions are very close in energy, however, it was possible to separate them in the $\gamma\gamma$ coincidence analysis, as will be shown below. The transition at 496(10) keV will also be further discussed below. Figure 2(b) shows enhancement of the 682- and 1510-keV transitions in comparison to the 570-keV transition for $M_\gamma = 1$, which suggests that those γ rays populate directly the ground state. The difference in intensity of the 570-keV transition between the $M_\gamma = 1$ and the $M_\gamma \leqslant 5$ spectra suggests that it most likely belongs to a cascade.
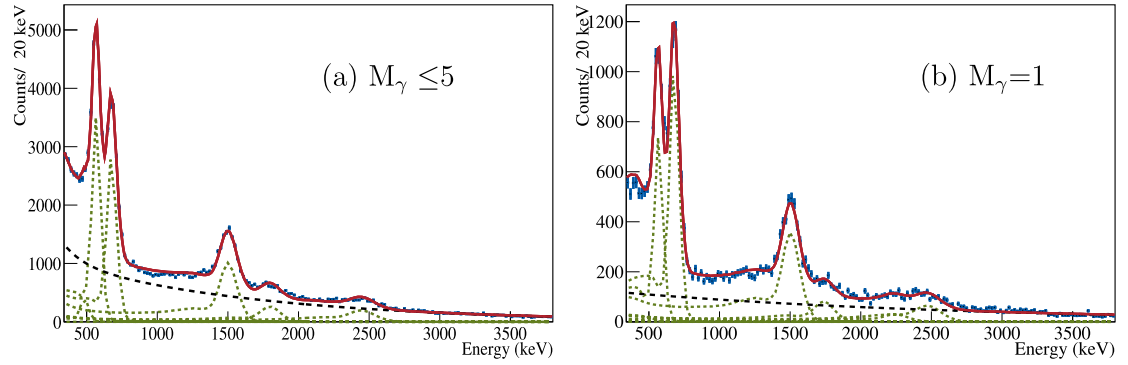
Figure 2. Doppler-corrected γ-ray spectra for the reaction ^{56}Sc$(p,pn)^{55}$Sc with add-back for (a) $M_\gamma \leqslant 5$ and (b) $M_\gamma = 1$. The green dashed lines represent the simulated γ-ray response functions of DALI2$^+$, the black dashed line is a double exponential fit to the background. The sum of all contributions is represented by the red line, whereas the blue points represent the experimental data.
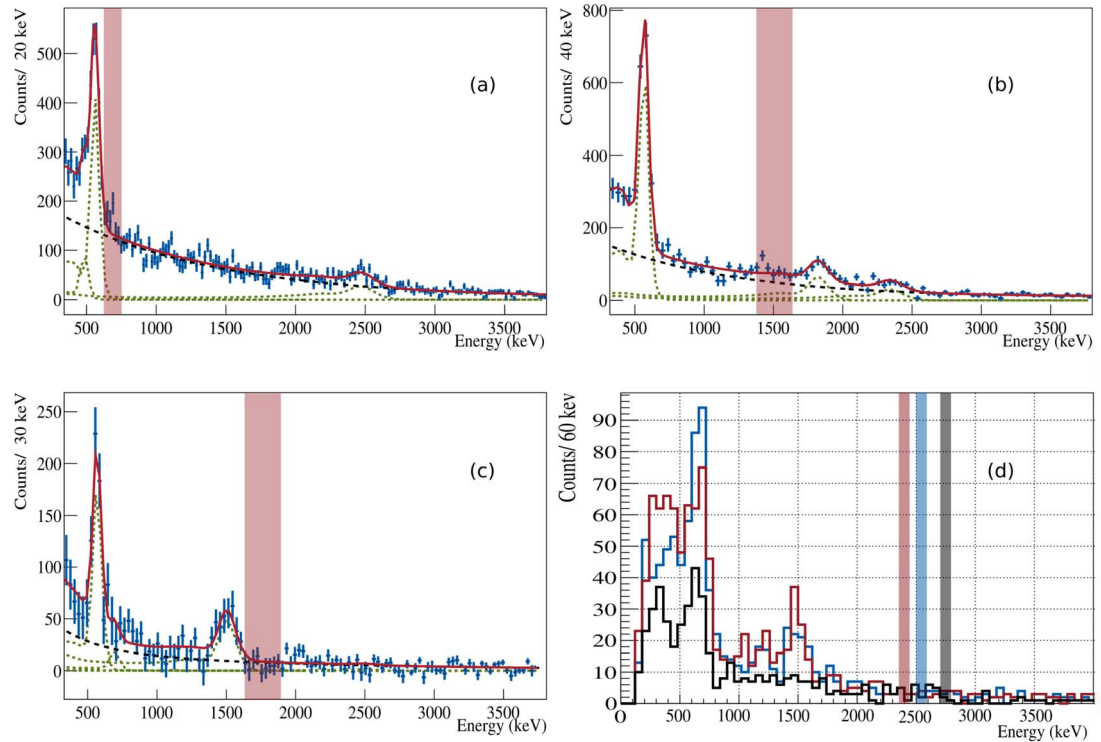

Figure 3. Doppler-corrected γ-ray spectra for the reaction ^{56}Sc$(p,pn)^{55}$Sc after applying energy gates. The colored areas show how the gate was chosen. Background has been subtracted for the spectra in panels (a), (b) and (c), while in panel (d) the background is plotted. Panel (a) shows the γ-ray spectrum in coincidence with the 682-keV line. Panel (b) shows the γ-ray spectrum in coincidence with the 1510-keV line. Panel (c) shows the γ-ray spectrum in coincidence with the 1780-keV transition. Panel (d) shows the γ-ray spectrum in coincidence with the 2345-keV peak (red color), the 2470-keV peak (blue color) and background (black color).

In order to construct a level scheme, a coincidence analysis was performed using the $M_\gamma \leqslant 5$ spectrum. γ-ray spectra after applying energy gates on the 682-, 1510-, and 1780-keV transitions, as well as the region around 2300-2500keV, are presented in figures 3(a), (b), (c) and (d), respectively. The gates applied are as follows - (a) 630 to 720 keV, (b) 1440 to 1560keV, (c) 1720 to 1860keV, (d) three gates with width of 60 keV with centers at 2330, 2500 and 2730keV. From figure 3(a) it can be seen that the 682-keV transition is in coincidence with the 570-keV and 2470-keV transitions. In addition, the transition at 496 keV is also present here. Figure 3(b) shows that the 1510-keV transition is in coincidence with a transition at around 570 keV as well as with the transition at 1780(36) keV with relative intensities of 100(6) and 44(5), respectively (relative intensity taken to the intensity of the 682-keV transition in each spectrum). The 1780 keV-transition gives back coincidences with the 570- and 1510-keV lines with the same relative intensity, as can be seen in figure 3(c). This puts those three transitions in a cascade, with the 1510-keV transition on the bottom, followed by the 570- and then 1780-keV transitions.
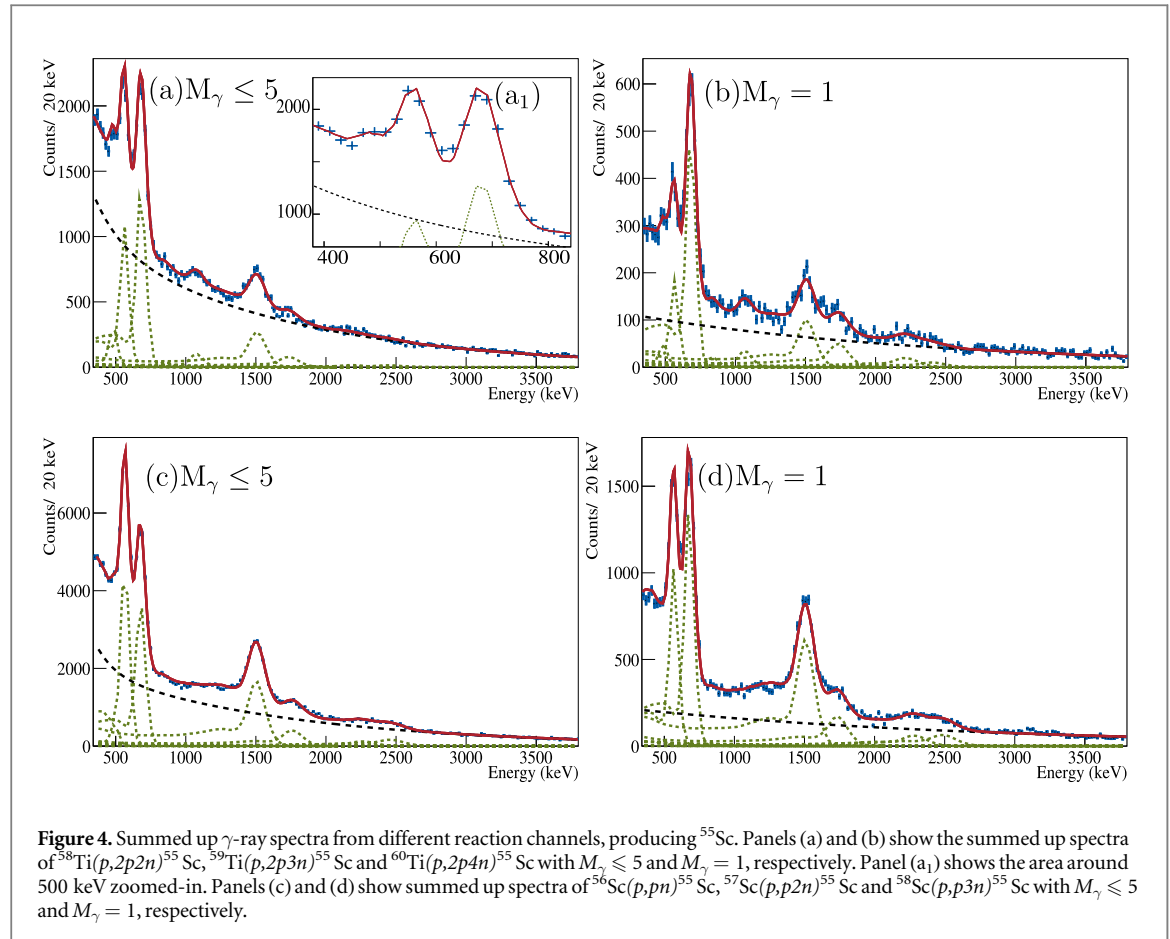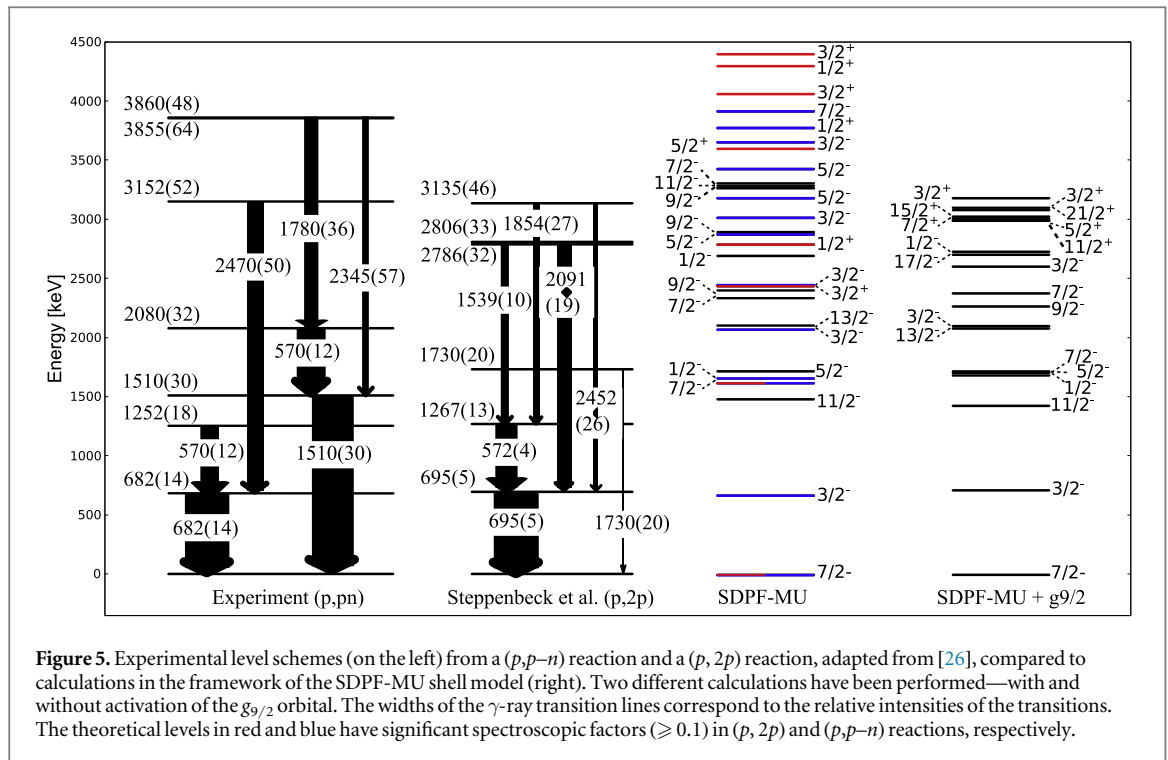
Figure 4. Summed up γ-ray spectra from different reaction channels, producing ^{55}Sc. Panels (a) and (b) show the summed up spectra of ^{58}Ti(*p,2p2n*)^{55} Sc, ^{59}Ti(*p,2p3n*)^{55} Sc and ^{60}Ti(*p,2p4n*)^{55} Sc with $M_\gamma \leqslant 5$ and $M_\gamma = 1$, respectively. Panel (a$_1$) shows the area around 500 keV zoomed-in. Panels (c) and (d) show summed up spectra of ^{56}Sc(*p,pn*)^{55} Sc, ^{57}Sc(*p,p2n*)^{55} Sc and ^{58}Sc(*p,p3n*)^{55} Sc with $M_\gamma \leqslant 5$ and $M_\gamma = 1$, respectively.

From the coincidence analysis it can be seen that the 682- and 1510-kev transitions are not in coincidence, supporting the conclusion that they show the decays of different levels directly to the ground state. The fact that the 682-keV transition as well as the 1510-keV transition are both in coincidence with the 570-keV peak points at it being a doublet. Otherwise, if the 570-keV line would be a single transition on top of the 1510-keV transition, which would then decay to the 682-keV state via an intermediate state, a strong transition at around 820 keV would be observed, which is not the case. The 2470-keV transition can only be seen in coincidence with the 682-keV transition, which places it directly on top of the former. A transition placed in the same manner and with the same energy (within uncertainty) was also reported in [26]. However, when gated on the area around 2400keV coincidences with both the 682- and 1510-keV peaks can be observed. It was determined that around 2400keV two transitions are present, which decay to the 1510- and 682-keV levels, respectively. Those have very similar energies and partially overlap, but from the coincidence spectra on figure 3(a) and (b) it can be observed that their centroids are different. The energies of 2345(57) and 2470(50) keV, have been determined from the coincidence spectra. Using those energies narrow gates have been performed on the two peaks and shown in figure 3(d), together with a gate on the background for comparison.

Additional non-direct reaction channels, producing ^{55}Sc, were also analyzed and are presented in figure 4, summed up. Panels (a) and (b) show summed-up nucleon-knockout reactions from Ti isotopes, all producing ^{55}Sc, with $M_\gamma \leqslant 5$ and $M_\gamma = 1$, respectively. Transitions at 570(12), 682(14), 1510(30), and 1780(36) keV can be observed, as well as additional transitions around 496 and 1100 keV. Here it can be observed that the ratio between the 682- and 570-keV peaks favors the higher-energy transition, not only in $M_\gamma = 1$ (like in figure 2(b)), but also in higher M_γ. Moreover, the transition at 496 keV can be distinguished in figure 4(a$_1$). The region between 486 and 582 keV was determined to be a triplet between a weak transition at 496(10) keV and a doublet at 570 keV of two γ rays with indistinguishable energies, sitting on top of the 682- and 1510-keV transitions, respectively. The region around 1100 keV was determined to contain two transitions, which were populated in different indirect reaction channels. Since statistics were limited, those transitions were not placed in the level scheme. Figure 4(d) and (e) show neutron-knockout reactions from heavier Sc isotopes. Peaks at 570(12), 682(14), 1510(30), 1780(36), and 2470(50) keV can be observed. No noticeable differences in the population of states is observed between the one- and multiple-neutron removal reaction channels. In the $M_\gamma = 1$ spectrum the transitions at 570, 682, and 1510keV have relative intensities of 51(1), 100(1), and 85(2), respectively. In the $M_\gamma \leqslant 5$ spectrum the same intensities are 105(3), 100(2), and 98(2), respectively.

Figure 5. Experimental level schemes (on the left) from a $(p,p-n)$ reaction and a $(p, 2p)$ reaction, adapted from [26], compared to calculations in the framework of the SDPF-MU shell model (right). Two different calculations have been performed—with and without activation of the $g_{9/2}$ orbital. The widths of the γ-ray transition lines correspond to the relative intensities of the transitions. The theoretical levels in red and blue have significant spectroscopic factors ($\geqslant 0.1$) in $(p, 2p)$ and $(p,p-n)$ reactions, respectively.

For all reaction channels inclusive cross sections have been obtained. They are presented in table 1. The transmission of ^{55}Sc (determined to be 53(1) %) along the beam line, which includes the efficiency of the beam line detectors and the reaction losses in the target, and the efficiency of MINOS for the detection of protons in the respective reaction channels were used for the calculation. The SAMURAI magnet has a large acceptance and all channels mentioned are well within it, so no correction is needed. The direct $(p, 2p)$ reaction channel was not available in this experiment due to the setting of the BigRIPS fragment separator, which cuts out ^{56}Ti from the incoming beam.

4. Discussion

The level scheme obtained for ^{55}Sc is shown in figure 5, left. The widths of the transition arrows represent the intensity of the γ rays in the $M_\gamma \leqslant 5$ spectrum. Based on the coincidence analysis, the 682- and 1510-keV transitions were placed decaying directly to ground state. The two transitions from the doublet at 570 keV were placed on top of the 682- and 1510-keV levels, respectively. The transition at 1780keV was placed on top of the 1510- and 570-keV transitions, since it comes in coincidence with both. The 2345-keV transition was placed on top of the 1510 keV level, while the 2470-keV transition is placed decaying to the 682-keV level. The two levels at 3855 and 3860keV are at the same energy, within uncertainty, however it cannot be confirmed if they are indeed the same state or not due to the high density of states. The transition at 496 keV, which can be seen in figure 4(a) and (a$_1$), has not been placed conclusively in the level scheme.

The suggested placement of the first excited state at energy of 682(14) keV agrees well with the one reported in literature at 695(5) keV [26]. This placement of the first excited state, which is much lower than the first 2^+ state in ^{54}Ca, cannot be explained by the $\pi f_{7/2} \bigotimes {}^{54}Ca(2^+_1)$ configuration. As suggested in [26], this would mean a rapid weakening of the N = 34 subshell closure with even one proton in the $\pi f_{7/2}$ orbital. Additionally, a transition at 572keV has also been reported previously, depopulating a state at 1267keV, which has been placed in a similar manner in our data. However, the 1510-keV line, which has been placed as decaying to ground state, has not been observed previously. A transition at similar energy of 1539(10) keV has been noted in [26], but it does not correspond to the one observed here, since if this was the case, it would be in coincidence with the transition at 682 keV.

The experimental data have been compared to calculations using the SDPF-MU shell-model effective interaction [39]. Full *sd* and *pf* model spaces were used for protons and neutrons, respectively, with effective charges of $e_\pi = 1.1e$ and $e_\nu = 0.1e$, which is very similar to the one used in [26], but considers also contributions of up to 4 particle-hole configurations in the wave function. The results are shown in figure 5. Spectroscopic factors have been calculated for the ^{56}Sc$(p,pn)^{55}$Sc and ^{56}Ti$(p,2p)^{55}$Sc reactions. For the (p,pn) reaction for ^{56}Sc a ground state with $J^\pi = 1^+$ was assumed, based on shell-model calculations [40] and supported by β-decay

Table 2. Theoretical spectroscopic factors (C^2S) for ^{56}Ti$(p,2p)^{55}$Sc one-proton removal reaction and ^{56}Sc$(p,pn)^{55}$Sc one-neutron removal reaction from the π and ν nlj orbitals. The spin-parity (J^π) and energy (E_γ) for the populated states in ^{55}Sc are given.

| | | ^{56}Ti$(p,2p)^{55}$Sc | | | | ^{56}Sc$(p,pn)^{55}$Sc | | | |
| | | C^2S | | | | C^2S | | | |
J^π	E [keV]	$\pi d_{5/2}$	$\pi d_{3/2}$	$\pi s_{1/2}$	$\pi f_{7/2}$	$\nu f_{7/2}$	$\nu f_{5/2}$	$\nu p_{3/2}$	$\nu p_{1/2}$
$7/2^-$	0				1.42		0.67		
$3/2^-$	670								0.8
$7/2^-_2$	1622				0.42		0.26		
$1/2^-$	1659								0.55
$3/2^-_2$	2071								0.37
$3/2^+$	2440		2.64						
$3/2^-_3$	2450							0.29	
$1/2^+$	2794			1.02					
$5/2^-_2$	2878						0.23		
$3/2^-_4$	3021						0.15		
$5/2^-_3$	3185						0.17	0.21	
$5/2^-_4$	3433							0.78	
$5/2^+$	3605	0.18							
$3/2^-_5$	3656							0.76	
$1/2^-_3$	3780							0.47	
$7/2^-_7$	3919						0.15		
$3/2^+_2$	4067		0.27						
$1/2^+_2$	4301			0.37					
$3/2^+_3$	4402		0.25						

systematics [41]. States populated in $(p, 2p)$ and (p,pn) reactions with spectroscopic factors larger than 0.1 have been highlighted in figure 5 in red and blue, respectively. These values are listed in table 2. The one-proton removal reaction is expected to populate positive parity states with significant spectroscopic factors, the highest population going to the first positive-parity state $J^\pi = 3/2^+$ at 2440keV. More states are expected to be strongly populated in the one-neutron removal reaction due to the many possible couplings of the neutron. The first excited state at 670 keV, as well as a $5/2^-$ and a $3/2^-$ states at around 3500keV are expected to be dominantly populated.

The calculated ground state of ^{55}Sc has spin-parity assignment (J^π) of $7/2^-$, which complies with the one suggested in [27, 41]. The first excited state is predicted at energy of 670keV with $J^\pi=3/2^-$, which agrees well (≈ 30 keV) with both literature and this work. It is then probable that the 682-keV state we observe is the first $J^\pi=3/2^-$ excited state. The observed second excited state at 1252keV is close in energy to the predicted theoretically $11/2^-$ state at around 1.5 MeV. However, $J^\pi = 11/2^-$ cannot be assigned to the 1252-keV state, since if this was the case no decay to the underlying $3/2^-$ state would be expected and rather a decay to the $7/2^-$ ground state. The 1252-keV state would better fit a $J^\pi = 1/2^-$, which is also what was suggested in [26].

The newly observed level at 1510keV, decaying directly to the ground state, would fit to the calculated $7/2^-_2$ state at an energy of 1622keV, since it is expected to decay with a strong M1 directly to ground state (B($M1$) = 0.0058 μ^2). The theoretical model, which includes excitations beyond the pf shell, calculates higher neutron occupation number of the $f_{5/2}$ orbital for the $7/2^-_2$ state as compared to the first excited state (1.19 and 1.03, respectively). In addition, the proton contributions to the wave function of the $7/2^-_1$ and $7/2^-_2$ states are very similar with occupation number of the $f_{7/2}$ orbital of 0.97, while the $3/2^-$ state has a notable contribution from the $p_{3/2}$ orbital with occupation number 0.15. In this sense the $7/2^-_2$ has a dominant neutron character. Additionally, this state is expected to be strongly populated in a neutron-knockout reaction (33% of the spectroscopic factor of the strongest populated state), but not so much (16% of the spectroscopic factor of the strongest populated state) in a proton-knockout, which would explain the fact that it was not observed in [26].

In our experiment a level at 3152 kev has been observed decaying to the first excited state with a γ ray at 2470 (50) keV. This is similar to the observed level at 3135(46) keV in [26]. However, this state was observed to decay to the 695- and 1267-keV states with very similar intensity. In contrast, in our data no transition to the 1252-keV state was observed. Therefore it is unlikely that the levels at 3152 and 3135 keV are one and the same, which is supported by the high density of states predicted in this energy region.

The effect of considering neutron excitations beyond the pf shell has been investigated by performing two calculations—with and without activation of the $g_{9/2}$ orbital. The calculation, excluding the $g_{9/2}$ orbital, has been used to predict a larger number of states, since it requires less computational time. Furthermore, it was also

used for the calculation of spectroscopic factors. The calculation including the $g_{9/2}$ has been limited to the first 10 positive parity and 10 negative parity states, producing results on the spin-parity J^π, level energies E_γ and reduced transition probabilities $B(E2)$ and $B(M1)$. Minor differences can be observed between the two calculations. The triplet of states around 1600 keV ($1/2^-$, $5/2^-$ and $7/2^-$) has different arrangement, as can be seen on figure 5. The same is valid for the doublet around 2100 keV ($3/2^-$ and $13/2^-$). Both calculations predict the first positive parity state to be $3/2^+$ state with similar energies ($\approx$150 keV difference). It can be concluded that the current manner of including the $g_{9/2}$ orbital does not present differences to the calculation in the original model space, to which the experimental data is sensitive. The energy placement of the low-lying states is satisfactory reproduced in both calculations. Conversely, excitations beyond the pf shell and the single particle energy of the $g_{9/2}$ orbital become relevant when going towards $N = 40$, as was shown in a recent work on Ca isotopes beyond $N = 34$ [42]. Further test would be the ability to reproduce the level schemes of heavier Sc isotopes, which will be addressed in an upcoming publication.

5. Conclusions

The neutron-rich ^{55}Sc was investigated via the one-neutron removal reaction and multinucleon removal reactions at the RIKEN Radioactive Isotope Beam Factory. Based on $\gamma\gamma$ coincidence analysis, a level scheme was constructed. It contains already reported excited states, as well as new ones. The experimental level scheme was compared to large-scale shell model calculations in the SDPF-MU framework. It can be assumed that the first excited state in ^{55}Sc has a spin-parity of $J_\pi = 3/2^-$ and energy of 682(14) keV, which agrees with previous suggestions that the $N = 34$ subshell closure breaks down even when only one proton occupies the $\pi f_{7/2}$ orbital. The experimental level at 1510(30) keV, not observed in previous studies, was tentatively assigned $J_\pi = 7/2_2^-$ due to its observed decay to ground state and the expected strong population in neutron-knockout reactions.

Acknowledgments

Data availability statement

The data cannot be made publicly available upon publication because they are owned by a third party and the terms of use prevent public distribution. The data that support the findings of this study are available upon reasonable request from the authors.

References

[1] Sorlin O and Porquet M G 2008 *Prog. Part. Nucl. Phys.* **61** 602–73
[2] Steppenbeck D *et al* 2013 *Nature* **502** 207–10
[3] Wienholtz F *et al* 2013 *Nature* **498** 346–9
[4] Huck A, Klotz G, Knipper A, Miehé C, Richard-Serre C, Walter G, Poves A, Ravn H L and Marguier G 1985 *Phys. Rev. C* **31** 2226–37
[5] Michimasa S *et al* 2018 *Phys. Rev. Lett.* **121** 022506
[6] Gade A *et al* 2006 *Phys. Rev. C* **74** 021302
[7] Chen S *et al* 2019 *Phys. Rev. Lett.* **123** 142501
[8] Otsuka T, Suzuki T, Fujimoto R, Grawe H and Akaishi Y 2005 *Phys. Rev. Lett.* **95** 232502
[9] Otsuka T 2013 *Phys. Scr.* **2013** 014007
[10] Nowacki F and Poves A 2009 *Phys. Rev. C* **79** 014310
[11] Hagen G, Hjorth-Jensen M, Jansen G R, Machleidt R and Papenbrock T 2012 *Phys. Rev. Lett.* **109** 032502
[12] Janssens R *et al* 2002 *Phys. Lett. B* **546** 55–62
[13] Dinca D C *et al* 2005 *Phys. Rev. C* **71** 041302
[14] Zhu S *et al* 2006 *Phys. Rev. C* **74** 064315
[15] Bürger A *et al* 2005 *Phys. Lett. B* **622** 29–34
[16] Prisciandaro J *et al* 2001 *Phys. Lett. B* **510** 17–23
[17] Steppenbeck D *et al* 2015 *Phys. Rev. Lett.* **114** 252501
[18] Rosenbusch M *et al* 2015 *Phys. Rev. Lett.* **114** 202501
[19] Liu H N *et al* 2019 *Phys. Rev. Lett.* **122** 072502
[20] Liddick S N *et al* 2004 *Phys. Rev. Lett.* **92** 072502

[21] Meisel Z *et al* 2020 *Phys. Rev.* C **101** 052801
[22] Iimura S *et al* 2023 *Phys. Rev. Lett.* **130** 012501
[23] Otsuka T, Gade A, Sorlin O, Suzuki T and Utsuno Y 2020 *Rev. Mod. Phys.* **92** 015002
[24] Nowacki F, Obertelli A and Poves A 2021 *Prog. Part. Nucl. Phys.* **120** 103866
[25] Leistenschneider E *et al* (The LEBIT Collaboration and the TITAN Collaboration) 2021 *Phys. Rev. Lett.* **126** 042501
[26] Steppenbeck D *et al* 2017 *Phys. Rev.* C **96** 064310
[27] Kumar P, Sarkar S, Singh P P and Raina P K 2019 *Phys. Rev.* C **100** 024328
[28] Fukuda N, Kubo T, Ohnishi T, Inabe N, Takeda H, Kameda D and Suzuki H 2013 *Nucl. Instrum. Methods Phys. Res., Sect. B* **317** 323–32 XVI International Conference on ElectroMagnetic Isotope Separators and Techniques Related to their Applications, December 2-7, 2012 at Matsue, Japan
[29] Kubo T *et al* 2012 *Prog. Theor. Exp. Phys.* **2012** 03C003
[30] Kumagai H, Ohnishi T, Fukuda N, Takeda H, Kameda D, Inabe N, Yoshida K and Kubo T 2013 *Nucl. Instrum. Methods* B **317**
[31] Kimura K *et al* 2005 *Nucl. Instrum. Methods* A **538** 608–14
[32] Obertelli A *et al* 2014 *Eur. Phys. J.* A **50** 8
[33] Santamaria C *et al* 2018 *Nucl. Instrum. Methods Phys. Res., Sect.* A **905** 138–48
[34] Kobayashi T *et al* 2013 *Nucl. Instrum. Methods* B **317** 294–304 16th International Conference on ElectroMagnetic Isotope Separators and Techniques Related to their Applications, December 2-7, 2012 at Matsue, Japan
[35] 2024 Ribf riken website, charged particle detectors data https://ribf.riken.jp/SAMURAI/index.php?ChargedParticleDetector
[36] Agostinelli S *et al* 2003 *Nucl. Instrum. Methods Phys. Res., Sect.* A **506** 250–303
[37] Takeuchi S, Motobayashi T, Togano Y, Matsushita M, Aoi N, Demichi K, Hasegawa H and Murakami H 2014 *Nucl. Instrum. Methods* A **763** 596–603
[38] Murray I *et al* 2018 *RIKEN Accel. Prog. Rep. vol 51* 158 https://nishina.riken.jp/researcher/APR/APR051/pdf/RIKEN_APR51.pdf
[39] Utsuno Y, Otsuka T, Brown B A, Honma M, Mizusaki T and Shimizu N 2012 *Phys. Rev.* C **86** 051301
[40] Liddick S N *et al* 2004 *Phys. Rev.* C **70** 064303
[41] Crawford H L *et al* 2010 *Phys. Rev.* C **82** 014311
[42] Chen S *et al* 2023 *Phys. Lett.* B **843** 138025